



# Pore-Throat Combination Types and Gas-Water Relative Permeability Responses of Tight Gas Sandstone Reservoirs in the Zizhou Area of East Ordos Basin, China

LI Mi<sup>1,2</sup>, GUO Yinghai<sup>1,2,\*</sup>, LI Zhuangfu<sup>1,2</sup>, WANG Huaichang<sup>3</sup> and ZHANG Jingxia<sup>1,2</sup>

<sup>1</sup> Key Laboratory of Coalbed Methane Resource and Reservoir Formation Process, Ministry of Education, Xuzhou 221008, Jiangsu, China

<sup>2</sup> School of Resources and Geosciences, China University of Mining & Technology, Xuzhou 221116, Jiangsu, China

<sup>3</sup> Research Institute of Petroleum Exploration & Development of Changqing Oilfield Company, PetroChina, Xi'an 710021, Shaanxi, China

**Abstract:** With the aim of better understanding the tight gas reservoirs in the Zizhou area of east Ordos Basin, a total of 222 samples were collected from 50 wells for a series of experiments. In this study, three pore-throat combination types in sandstones were revealed and confirmed to play a controlling role in the distribution of throat size and the characteristics of gas-water relative permeability. The type-I sandstones are dominated by intercrystalline micropores connected by cluster throats, of which the distribution curves of throat size are narrow and have a strong single peak (peak ratio >30%). The pores in the type-II sandstones dominantly consist of secondary dissolution pores and intercrystalline micropores, and throats mainly occur as slice-shaped throats along cleavages between rigid grain margins and cluster throats in clay cement. The distribution curves of throat size for the type-II sandstones show a bimodal distribution with a substantial low-value region between the peaks (peak ratio <15%). Primary intergranular pores and secondary intergranular pores are mainly found in type-III samples, which are connected by various throats. The throat size distribution curves of type-III sandstones show a nearly normal distribution with low kurtosis (peak ratio <10%), and the micro-scale throat radii (>0.5 μm) constitute a large proportion. From type-I to type-III sandstones, the irreducible water saturation ( $S_{wo}$ ) decreased; furthermore, the slope of the curves of  $K_{rw}/K_{rg}$  in two-phase saturation zone decreased and the two-phase saturation zone increased, indicating that the gas relative flow ability increased. Variations of the permeability exist in sandstones with different pore-throat combination types, which indicate the type-III sandstones are better reservoirs, followed by type-II sandstones and type-I sandstones. As an important factor affecting the reservoir quality, the pore-throat combination type in sandstones is the cumulative expression of lithology and diagenetic modifications with strong heterogeneity.

**Key words:** tight gas sandstone, pore-throat combination type, throat characteristic, gas-water relative permeability, Zizhou area, Ordos Basin

Citation: Li et al., 2019. Pore-Throat Combination Types and Gas-Water Relative Permeability Responses of Tight Gas Sandstone Reservoirs in the Zizhou Area of East Ordos Basin, China. *Acta Geologica Sinica* (English Edition), 93(3): 622–636. DOI: 10.1111/1755-6724.13872

## 1 Introduction

The development of unconventional oil and gas has to some extent changed the global energy structure. Tight sandstone gas accounts for a high proportion of China's unconventional gas, which plays an important strategic role in a rapid development stage (Zou et al., 2015; Jia et al., 2016). Different from conventional sandstone reservoirs, tight gas sandstones have a significant feature of low porosity and low permeability, which consist of micro- to nanoscale pore throat systems characterized by various types, complex structures, highly differentiated connectivity and strong heterogeneities (Higgs et al., 2007; Rezaee et al., 2012; Er et al., 2015; Wu et al., 2017). The micro- to nanoscale pore throat structures directly affect the storage space and permeability of the reservoir (Li et al., 2017; Wu et al., 2018). In particular, the throat

characteristic is a vital factor affecting the properties of reservoir permeability (Xiao et al., 2017). Under the constraints of the strong heterogeneities of the microstructure and the research technology, there are few systematic studies of pore throat structures in tight gas sandstones and correlation studies between microstructure and macroscopic properties of reservoir permeability (Algiveet et al., 2012; Xi et al., 2016). Therefore, investigating the distribution, characteristics and combination types of pores and throats and discussing their influences on permeability are significant for reservoir evaluation and understanding the distribution and accumulation of tight gas.

The study of pore throat characteristics in tight sandstone reservoirs has become a research focus. The types, origin, morphology, sizes and distribution of pores have been the focus of researchers through various methods and techniques, such as direct observation (e.g.,

\* Corresponding author. E-mail: gyhai@163.com

SEM and X-ray micro-computed tomography), quantitative measurement (e.g., high pressure mercury intrusion) and the application of fractal theory (Hu et al., 2012; Giri et al., 2012; Bai et al., 2013; Ge et al., 2015; Dou et al., 2017; Liu et al., 2017). Inspections through thin-section petrography and SEM are universally used to qualitatively or semi-quantitatively describe pore throat structures (Pittman, 1992), which can provide information about the shapes, sizes, positions and diagenetic evolution. In recent years, the improvements of research technology, especially the application of RCP promote the further study of throats. Researchers have carried out research on the reservoir evaluation and formation mechanism through various characterization parameters of throats (Pittman, 1992; Nelson, 2009; Deng et al., 2011; Xiao et al., 2016). Although limitations of the lower intrusion pressure cause RCP to be unable to measure the pores and throats that are smaller than 0.12  $\mu\text{m}$ ; RCP can be used to effectively separate pores and throats and reveal the sizes and distribution of throats (Zhao et al., 2015; Xi et al., 2016). Researchers often use the throat size or shape to classify throat types. According to the size, the throats have been divided into micropore throats (diameter less than 1  $\mu\text{m}$ ), mesopore throats (diameter between 1 and 10  $\mu\text{m}$ ) and macropore throats (diameter greater than 10  $\mu\text{m}$ ) (Nelson, 2009). Based on the shape, throats can be divided into pore-shrinking throats, neck-contracted throats, slice-shaped throats and cluster throats (Yu, 2009). The throat types in tight sandstone reservoirs are complex and diverse; however, few studies have studied the characteristics and influencing factors of each kind of throat. Therefore, the systematic study of pores and throats to further understand the microstructure of tight gas sandstone reservoirs is required.

Sedimentation and subsequent diagenesis are the dominant factors affecting the pore throat structures of sandstone reservoirs (Lander and Walderhaug, 1999). Sedimentary processes further influence the diagenesis by controlling lithology parameters, such as grain component, content, size, sorting and shape (Lv and Liu, 2009; Ajdukiewicz and Lander, 2010; Yu et al., 2018). A complicated microstructure is the result of prolonged diagenetic modifications with the change in pore-throat type, size and distribution (Morad et al., 2010; Lai et al., 2015). Compaction and cementation reduce the primary reservoir spaces and decrease the pore-throat sizes (Hill and Collen, 1978). Dissolution that forms secondary dissolved pores to increase the pore-throat radius improves the physical properties (Liu et al., 2016). Therefore, the pore-throat structure is interpreted as the result of diagenetic evolution affected by sedimentary parameters (Sheng et al., 2018), which means there are certain regular patterns to be found in the study of the combination types of pores and throats. In addition, the study is fundamental for tight gas sandstone reservoir evaluation.

The percolation, distribution and displacement efficiency of the fluid flow in the core is affected and controlled by the pore-throat structure (Chalmers et al., 2012). The irreducible water saturation in tight gas sandstones is universally high and variable (Spencer, 1985), of which the degree affects the reservoir

exploitation mode and productivity. The exploitation of tight gas is a process of gas-water two-phase dynamic change; thus, investigating relative permeability has more practical significance for tight gas exploitation. Crucial properties in the research of gas-water relative permeability are the capillary pressure and relative permeability curves (Teige et al., 2006), which can be directly obtained through laboratory experiments from steady-state or unsteady-state techniques (Shanley et al., 2004; Bultreys et al., 2016; Zhang et al., 2017). In tight gas sandstones with complex and multiple-scale pore-throat structures, the characteristics of two-phase fluid flow strongly deviate from conventional sandstones (Shanley et al., 2004; Bultreys et al., 2016), but the impacts of pore-throat structures on gas-water relative permeability have been rarely studied. Consequently, a deep understanding of the gas-water relative permeability response to different pore-throat combination types is important for tight gas exploitation.

In this study, the 222 tight gas sandstone samples were selected from Upper Paleozoic gas-bearing layers (the third section of the Shan 2 member and the upper section of the He 8 member) in the Zizhou area, Ordos Basin. Porosity and permeability data were collected from the Research Institute of Petroleum Exploration & Development of Changqing Oilfield Company, PetroChina. Thin-section petrography, SEM, RCP and gas-water relative permeability tests were used to reveal the characteristics of pore-throat and the gas-water relative permeability of the samples. The detrital mineralogy and pore-throat combination types of the samples were studied based on the thin-section petrography. Nine samples were selected for SEM, RCP and gas-water relative permeability tests to investigate the pore throat sizes and gas-water relative permeability in samples with different pore-throat combination types. Furthermore, the effects of pore-throat combination types of sandstones on the gas-water relative permeability were analyzed. And the diagenetic control on pore-throat combination types of sandstones was discussed.

## 2 Geological Setting

The Ordos Basin, the second largest sedimentary basin in China, is located in the central part of the China plate (Dai et al., 2005; Tang et al., 2014; Ding et al., 2016). It belongs to a multicyclic superimposed basin after multiple tectonic movements during its prolonged evolution over geological time (Yang et al., 2005). Based on the structural characteristics and evolutionary history, it is subdivided into six first-order structural units (Fig. 1; Ji et al., 2010). Overlaying the Archean and Proterozoic metamorphic crystalline rock basement, cap rocks from the Paleozoic to Cenozoic were deposited in the Ordos Basin, and the Upper Paleozoic is the major gas bearing system with abundant gas exploration prospects (Li et al., 2017).

The Zizhou area is located in the Yishan Slope, which is the largest structural unit in the middle of the Ordos Basin (Fig. 1). There are large tight sandstone gas fields distributed in the Yishan Slope, such as Sulige and Yulin

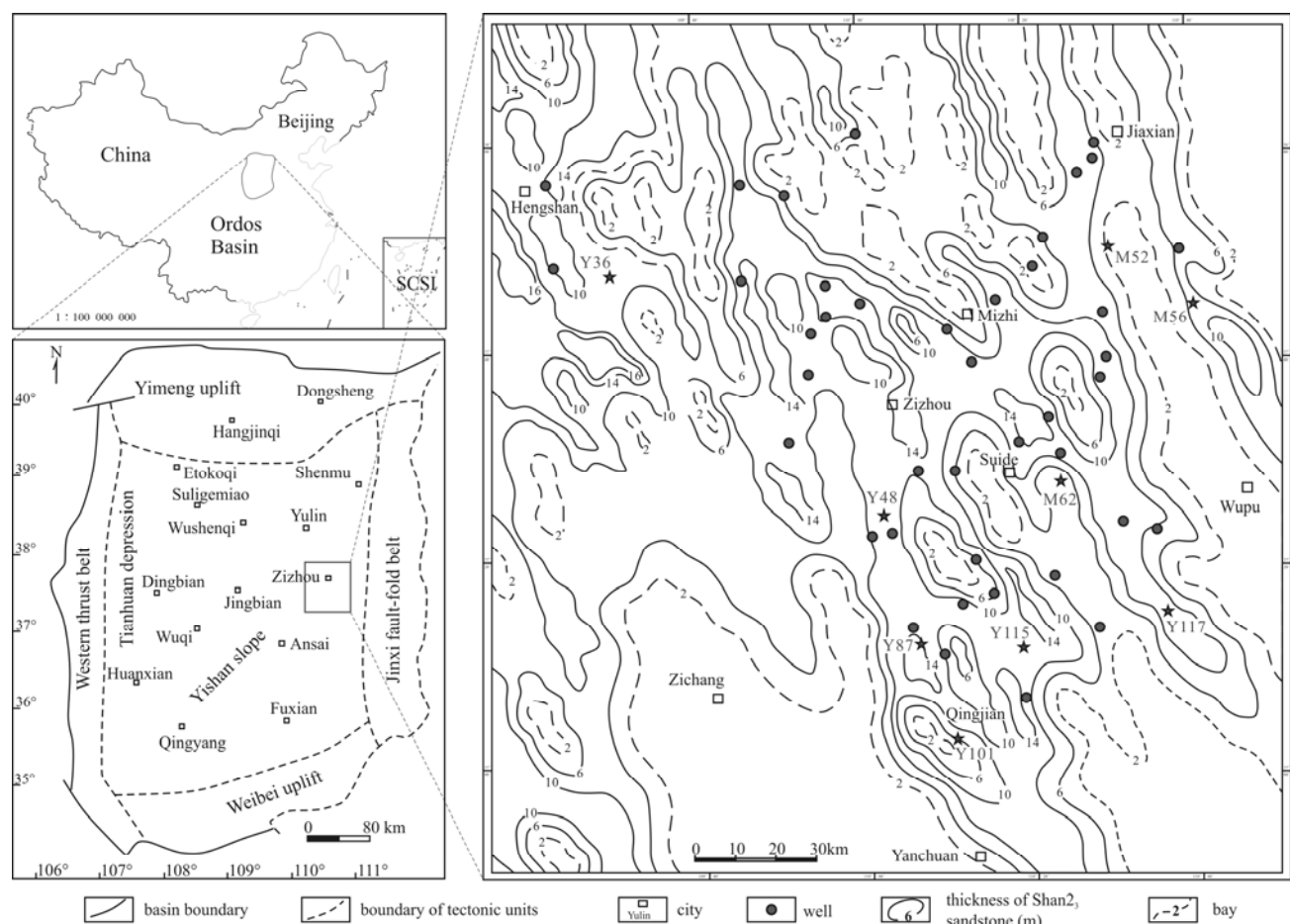


Fig. 1. Map showing structural units and location of the Zizhou area in the east Ordos Basin, China, and the thickness distribution in the Shan 2<sub>3</sub> section sandstones. The 222 core samples were collected from the 50 wells in the Zizhou area.

(Cao et al., 2011; Zou et al., 2018). During the Late Paleozoic, a set of coal-bearing continental clastic rocks with multiple gas-bearing layers was deposited in the study area: Benxi Formation (C<sub>2b</sub>), Taiyuan Formation (P<sub>1t</sub>), Shanxi Formation (P<sub>1s</sub>), Xiashihezi Formation (P<sub>2x</sub>), Shangshihezi Formation (P<sub>2s</sub>) and Shiqianfeng Formation (P<sub>2sh</sub>). The Shanxi Formation and Xiashihezi Formation, which were deposited in shallow sand-rich deltas (Shan et al., 2018) and mainly consist of sandstones, mudstones and coals, can be divided into 2 and 4 members, respectively.

3 Samples and Experimental Methods

3.1 Samples

The third section of the Shan 2 member and the upper

section of the He 8 member are the major gas-bearing layers of the Upper Paleozoic tight gas reservoirs in Zizhou area. The 222 samples were collected from 50 wells in the Zizhou area (Fig. 1) for thin-section petrography observation. The 119 samples were collected from the third section of the Shan 2 member, and the 103 samples were collected from the upper section of the He 8 member. Based on the petrography, porosity and permeability data of the sandstones, nine representative samples were selected for RCP and gas-water relative permeability experiments (Table 1). The nine samples were collected from the nine wells in the depth interval 1992.45–2924.58 m. Samples 1, 2, 6 and 9 were collected from the third section of the Shan 2 member, and the others were collected from the upper section of the He 8

Table 1 Wells, depth, porosity, permeability and lithology of the nine samples in the Zizhou area

| Type | Samples | Wells | Depth (m) | Porosity (%) | Permeability (mD) | Lithology                     |
|------|---------|-------|-----------|--------------|-------------------|-------------------------------|
| I    | S1      | Y117  | 2294.16   | 2.75         | 0.0167            | medium-grained litharenite    |
| I    | S2      | Y101  | 2354.46   | 8.8          | 0.214             | coarse-grained litharenite    |
| I    | S3      | M52   | 2116.84   | 7.2          | 0.232             | coarse-grained sublitharenite |
| II   | S4      | M62   | 2181.59   | 9.1          | 0.3363            | coarse-grained quartz arenite |
| II   | S5      | Y115  | 2157.58   | 6.46         | 0.4406            | medium-grained sublitharenite |
| II   | S6      | M56   | 1992.45   | 9.1          | 0.454             | medium-grained sublitharenite |
| III  | S7      | Y36   | 2924.58   | 7.03         | 0.5534            | medium-grained quartz arenite |
| III  | S8      | Y87   | 2371.59   | 8.96         | 0.618             | coarse-grained quartz arenite |
| III  | S9      | Y48   | 2589.19   | 5.9          | 0.892             | coarse-grained quartz arenite |

member. The porosity of the samples ranges from 2.75% to 9.1% and the permeability is in a range of 0.0167 mD to 0.8920 mD (Table 1).

### 3.2 Experimental methods

The 222 samples are core plugs drilled from the wells parallel to the horizontal direction of the sandstone cores. The samples were polished for the thin section with red epoxy resin to highlight the pores for polarized light microscopy observation. The thin sections were partly stained with alizarin red for carbonate mineral determination. The maximum resolution of the polarized light microscopy is 0.2  $\mu\text{m}$ , which can effectively identify the micron-scale and some submicron-scale pore-throats.

The nine samples are ~6 cm long and ~2.5 cm in diameter. Each core plug was divided into four parts, of which three parts with lengths of ~0.5 cm, ~0.5 cm and ~4 cm were for SEM, RCP and gas-water relative permeability experiments, respectively. The residual part was polished for the thin section. To further observe the nanometer-scale and submicron-scale pore-throats, high-resolution SEM imaging of 3 nm was performed on the gold-coated and dried sample surfaces using an FEI Quanta TM 250 in the Advanced Analysis and Computation Center of the China University of Mining and Technology. RCP and gas-water relative permeability experiments were performed in the Petroleum Exploration and Development Research Institute, Langfang branch, China. RCP was tested at the rate of 0.00005 ml/min in an ASPE-730 mercury porosimeter following the Chinese standard Q/SY DQ1526-2012, in which the maximum intrusion pressure is 900 psi, corresponding to a pore-throat radius of 0.12  $\mu\text{m}$ . However, due to errors in the sample preparation, only seven samples were chosen for the gas-water relative permeability experiment. The gas-water relative permeability experiment was performed in an HBXS-2 relative permeameter using the unsteady-state method following the Chinese standard GB/T 28912-2012. The water phase permeability ( $K_w$ ) was measured first after saturating the dried core with formation water and then displacing the water with gas under rate-controlled pressure.

## 4 Results

### 4.1 Detrital mineralogy

Point counting of 222 thin-sections reveals that the sandstones is mainly quartz arenites (36%) and sublitharenites (57%) according to Folk's classification scheme (Folk, 1980), with an average composition of  $Q_{88.58}F_{0.16}R_{11.26}$  (Fig. 2). The samples are feldspar poor and lithic rich. Point counting data show that the most common lithic are metamorphic fragments (av. 4.94%), altered fragments (av. 2.42%) and volcanic fragments (av. 1.59%). The sandstones are primarily medium-to coarse-grained and moderately to well-sorted. The grain contacts are mostly linear to concavo-convex contacts.

### 4.2 Reservoir quality

The sandstones in the Zizhou area with porosity ranging from 0.68% to 6.4% and permeability ranging from

0.0088 mD to 1.5492 mD (only seven samples are >1 mD). Thus, the sandstones are documented as typical tight reservoirs. Figure 3 shows the positive correlation between the plug porosity and permeability.

### 4.3 Pore-throat combination types

The pores of the samples observed in thin-section and SEM analysis were classified into four types: (a) primary intergranular pores referring to original depositional spaces between detrital grains, (b) secondary intergranular pores consisting of the partial dissolution of detrital grains along grain margins and the partial to pervasive dissolution of tephra as intergranular matrix, (c) secondary intragranular pores consisting of a selective dissolution of grain interior and grain-mold dissolution showing characteristic outlines of the precursor grains, and (d) intercrystalline micropores in clay minerals referring to kaolinite, illite-smectite, illite and chlorite. The throats observed in samples were divided into pore-shrinking throats, neck-contracted throats, slice-shaped throats and cluster throats based on the shape according to the classification adopted from Yu (2009) (Fig. 4).

In previous studies, it has been reported that there is a

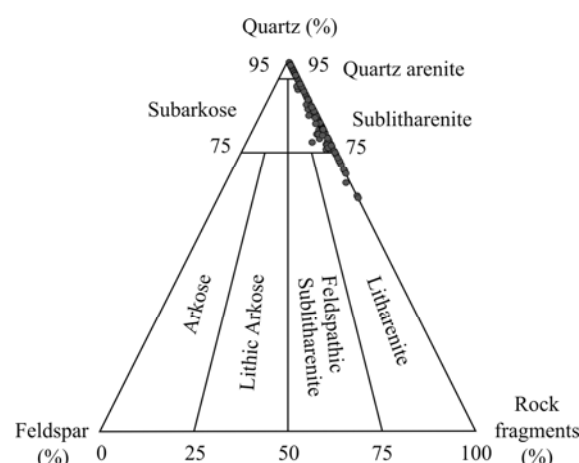


Fig. 2. QFL detrital composition of the samples in the Zizhou area plotted on Folk's (1980) ternary diagram.

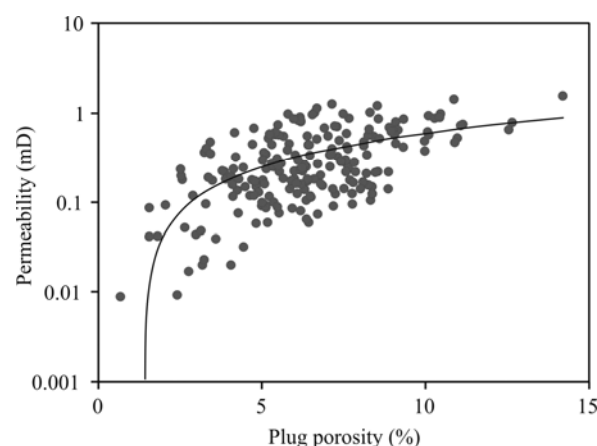


Fig. 3. Plot showing the relationship between the plug porosity and the permeability of the samples in the Zizhou area.

certain regular pattern of various pores in sandstones (Liu et al., 2018). Based on the thin-section observation of the 222 samples, we found there are three pore-throat combination types in tight gas sandstones in the Zizhou area (Table 2), and variations in the reservoir quality exist in sandstones with different pore-throat combination types. Figure 5 shows the porosity and permeability distribution of three types of sandstones, and the differences in the permeability distribution is significant, indicating the reservoir quality of type-III sandstones are better (permeability > 0.3 mD), followed by type-II sandstones (0.1 mD < permeability < 0.5 mD) and type-I sandstones (permeability < 0.3 mD).

The type-I samples are dominated by intercrystalline micropores connected by cluster throats (Table 2). Intercrystalline micropores observed by thin section and SEM analysis mainly occur in clay minerals of authigenic or altered origin, which cannot be clearly distinguished from the throats (Figs. 6a, b, c) (Xiao et al., 2017). These throats were classified into cluster throats characterized as microscale, cross-capillary and complicated (Yu, 2009).

The pores in type-II sandstones dominantly consist of secondary dissolution pores and intercrystalline micropores (Table 2), and the proportion of secondary intragranular pores is relatively high. Throats found in type-II sandstones mainly occur as two states: slice-shaped throats along cleavages between the rigid grain margins and cluster throats in clay cement (Table 2).

Secondary intragranular pores observed in samples have the characteristics of isolated distribution and poor connectivity (Fig. 6d). Due to the low dissolution degree, the content of secondary intergranular pores is low and the radius is small. Moreover, the dissolved spaces were generally filled with authigenic clay minerals during the

diagenetic period (Fig. 6e). The throats occur as slice-shaped with the filling of euhedral quartz and as cluster throats with the filling of clay minerals (Figs. 6e, f).

Primary intergranular pores and secondary intergranular pores are mainly found in type-III samples (Table 2), and the throat types are various. The pores were generally connected by slice-shaped throats occurring as cleavages between the rigid grain margins with radii of 2  $\mu\text{m}$  (Figs. 6h, i). Occasionally, pore-shrinking and neck-contracted throats with radii ranging from 3  $\mu\text{m}$  to 4  $\mu\text{m}$  (Fig. 6h) are visible in secondary intergranular pores due to the strong dissolution. In addition, the cluster throats occurred with radii ranging from 0.5  $\mu\text{m}$  to 2  $\mu\text{m}$  when the clay minerals filling in the pores (Figs. 6i, l). As tephra-dissolution pores are well developed in samples with strong dissolution, the throats are present mainly in three forms: (1) pore-shrinking throats with the largest radius of 29  $\mu\text{m}$ ; (2) neck-contracted throats between grains in point contact with the radius of 10  $\mu\text{m}$ ; (3) slice-shaped throats between grains in line and concave-convex contact with radii ranging from 5  $\mu\text{m}$  to 15  $\mu\text{m}$  (Figs. 6j, k).

#### 4.4 Pore-throat size and distribution

Nine samples were selected as representative of three pore-throat combination types for RCP test. The pore types and thin-section porosity of the nine representative samples are shown in Fig. 7. The sizes and distribution curves of the pore, throat and pore-throat radius ratio obtained from the RCP data of the nine samples are shown in Fig. 8 and Fig. 9. The pore radius distribution ranges of the samples are quite different; however, the average pore radii tend to have an interval of 127.3–181.38  $\mu\text{m}$  with smaller differences (Fig. 8). The average throat radii of the samples range over one order of magnitude from 0.3 to 6.5

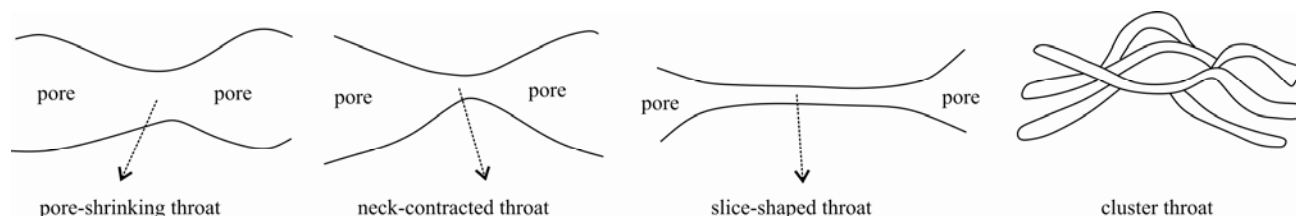


Fig. 4. Throat classification plot adopted from Yu (2009).

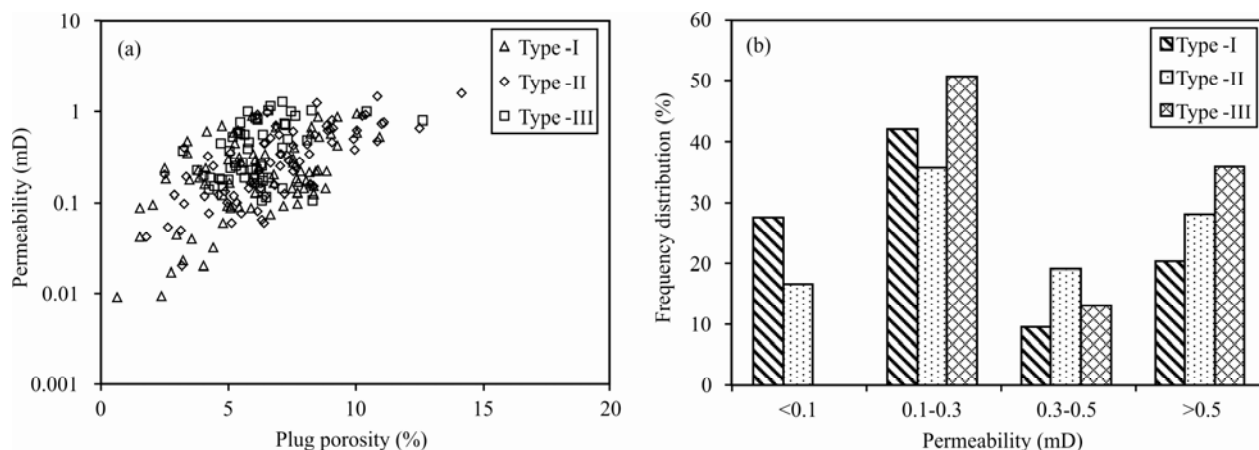


Fig. 5. Plot showing the distribution of porosity and permeability of sandstones with different pore-throat combination types in the Zizhou area.



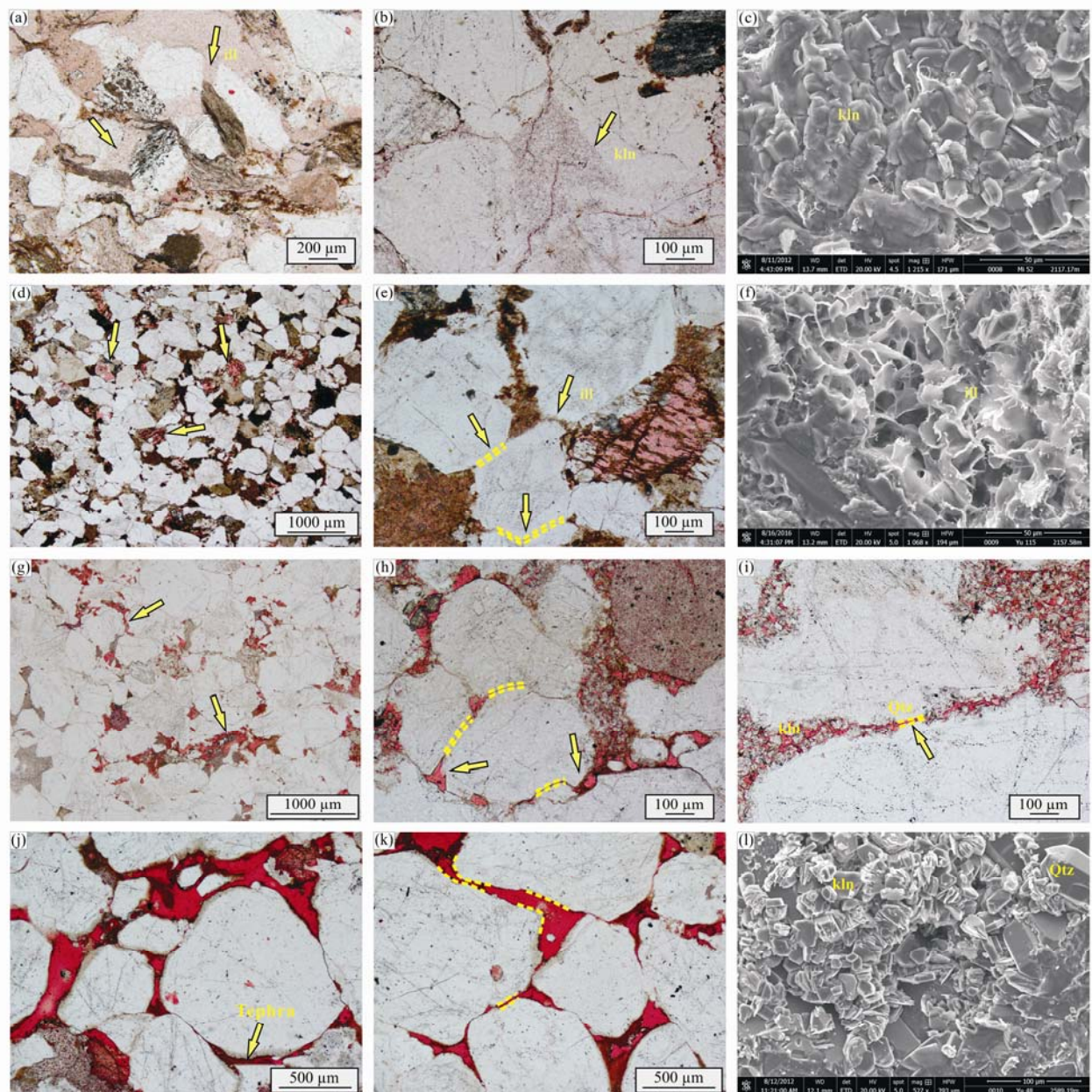


Fig. 6. Photomicrographs showing the pores and throats in sandstones in Zizhou area.

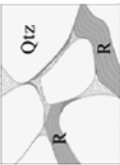

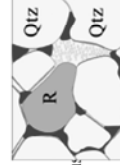
(a) Inter-crystalline micropores occur in illite with cluster throats (S1); (b) Inter-crystalline micropores occur in kaolinite with cluster throats (S3); (c) From SEM, kaolinite occurs as booklets and vermicular aggregates with cluster throats (S3); (d) Secondary intragranular pores occur with poor connectivity (S6); (e) The slice-shaped throats occur along cleavages between the rigid grain margins and cluster throats occur in clay cement (S6); (f) From SEM, the altered illite with honeycomb-like pores generally fills the secondary intergranular pores (S5); (g) Secondary intergranular pores with good connectivity (S7); (h) Primary intergranular and secondary intergranular pores occur at larger sizes (S9); (i) The slice-shaped throats occur in cleavages between the rigid grain margins, which change to be cluster throats due to the cementation of kaolinite (S9); (j) Tephra in sandstone are strongly dissolved and form dissolution pores with various types of throats (S8); (k) Neck-contracted and slice-shaped throats occur between grains in sandstone (S8); (l) Authigenic kaolinite and quartz with euhedral-granular texture filling in the intergranular pores (S8).

μm (Fig. 8).

The pore radius distribution curves look similar with approximate peak centers (Fig. 9a). However, the throat size and pore-throat radius ratio distribution curves exhibit significant differences (Figs. 9b, 9c). The differences in the accentuation of pore-throat radius ratio are related to the throat properties, implying that the characteristics of the throat might be the key factor controlling the

heterogeneity of the microstructure in tight sandstones. The distribution curves of the ratio of pore size to throat size show a substantial inverse correlation with the throats (Fig. 9c). For example, when the peak value of the throat radius (6.5 μm) is larger in sample 5, the value of the pore-throat radius ratio (55.36) is smaller. This fact proves that throat size plays a dominant role in the pore-throat structure.

Table 2 Summary of pore-throat combination types in sandstones in the Zizhou area

| Pore-throat combination types code | Pore types   | Throat types         | Thin-section photography  | Common lithology               | Diagenetic alteration   | Throat radius distribution curves  | Gas-phase relative permeability curves  | $S_{wo}$ | Reservoir quality                             |
|------------------------------------|--|----------------------|---|--------------------------------|---|--|---|----------|---|
| I                                  | Intercrystalline micropores                                | Cluster              |  | Medium-grained sublitharenites | Primary porosity lost by strong compaction. Common clay cementation.  | Narrow with high single kurtosis (>30%).   | An approximately linear shape.  | High     | None-Low ( $K < 0.3$ mD)                      |
| II                                 | Secondary dissolution pores, intercrystalline micropores   | Slice-shaped throats |  | Coarse-grained sublitharenites | Primary porosity lost by strong compaction. Common detrital grains internal dissolution. Cementation by quartz and clay minerals that fills the pore spaces. Small amount of primary pores reserved after compaction. | A bimodal distribution with a substantial low-value region between the peaks (<15%). | A shape changed from concave to linear with the decrease in water saturation. | Medium   | Low ( $0.1 \text{ mD} < K < 0.5 \text{ mD}$ ) |
| III                                | Primary intergranular pores, secondary intergranular pores | Various              |  | Coarse-grained quartz arenites | Dissolution of detrital grains and matrix. Common quartz overgrowth cementation.  | A nearly normal distribution with low kurtosis (10%).                                | A concave shape.  | Low      | Low-Good ( $0.3 \text{ mD} < K$ )             |

Note: K, permeability; Qtz, Quartz; R, rock fragments.

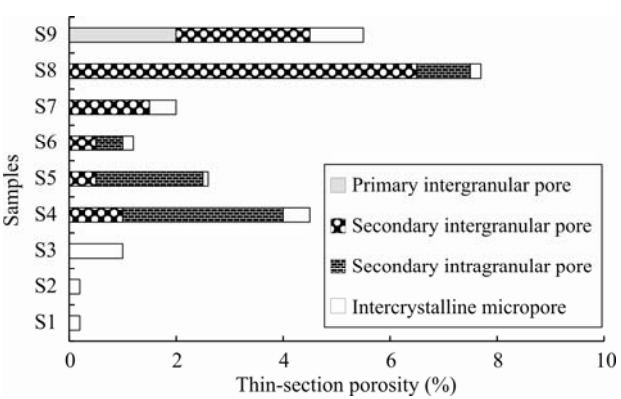


Fig. 7. Pore types and thin-section porosities estimated for each sample.

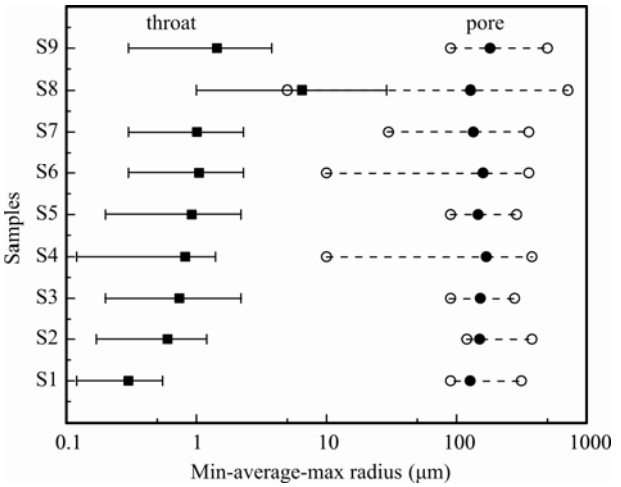


Fig. 8. The min-average-max radius of the pore and throat derived from the RCP data of the nine samples.

Figure 10 shows the throat radius distribution curves derived from the RCP of nine samples. There are significant differences in throat radius, size range and central tendency of the three types of sandstones. Type-I is represented by sample 1, 2 and 3, and the curve distribution is narrow with high single kurtosis (>30%) (Fig. 10a). The peak in the type-I curves corresponds to cluster throats in sandstones with radii ranging from 0.2  $\mu\text{m}$  to 0.5  $\mu\text{m}$ . Type-II is represented by sample 2, 3 and 4, of which the curves show a bimodal distribution with a substantial low-value region between the peaks (Fig. 10b). The percentages of the peaks are less than 15%. The left peak of type-II curves corresponds to the cluster throats with radii ranging from 0.2  $\mu\text{m}$  to 0.5  $\mu\text{m}$  and the right peak corresponds to slice-shaped throats with radii larger than 0.5  $\mu\text{m}$ . There are multiple types of throats with the larger size in type-III sandstones. Type-III is represented by sample 7, 8 and 9, of which the curves are in a nearly normal distribution with low kurtosis (10%), larger spread and better continuity (Fig. 10c). And the micron-scale throat radii (>0.5  $\mu\text{m}$ ) occupy a large proportion in type-III curves.

4.5 The gas-water relative permeability

Seven samples were chosen as representative of three

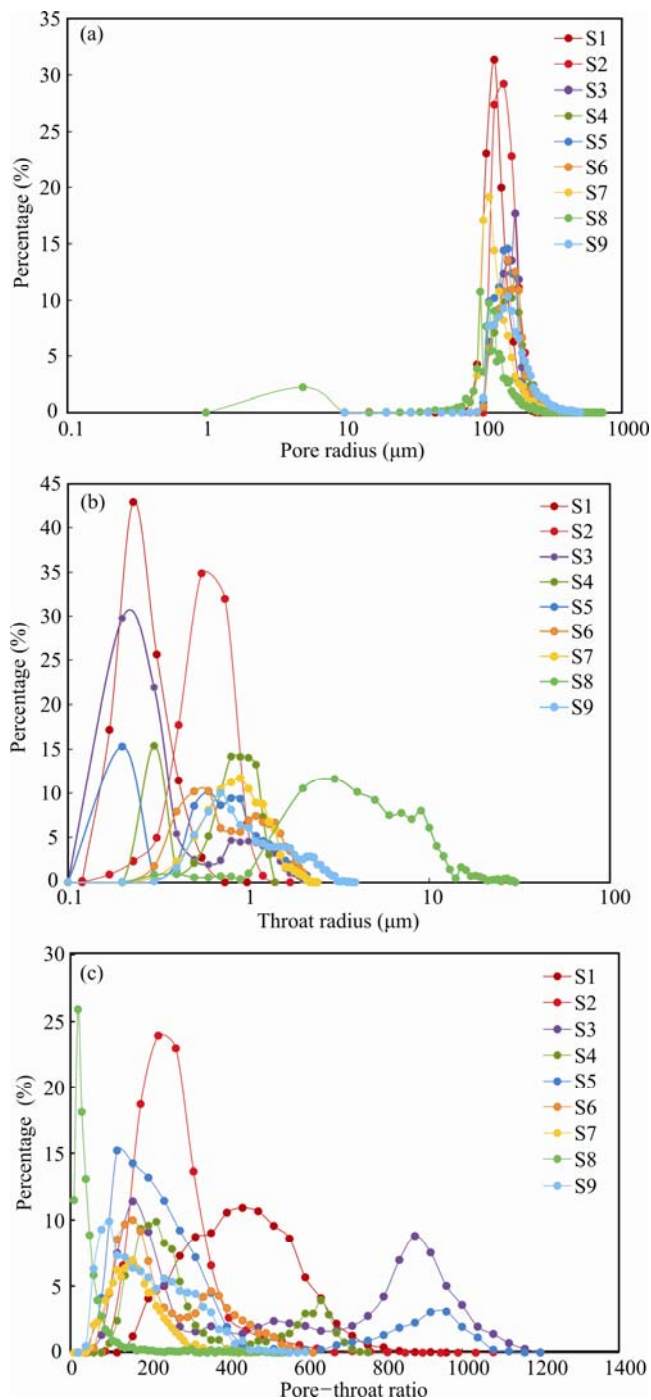


Fig. 9. The pore radius, throat radius and pore-throat ratio distribution derived from the RCP data of the nine samples. (a) Pore radius distribution curves; (b) throat radius distribution curves; (c) pore-throat ratio distribution curves.

pore-throat combination types for the gas-water relative permeability experiment. The basic data of the samples show that the  $S_{wo}$  decreases and the range of the two-phase saturation zone increases from type-I sandstones to type-III sandstones (Table 3).

The gas-water relative permeability curves of the samples are shown in Fig. 11. The water-phase relative permeability curves are similar with concave shapes.

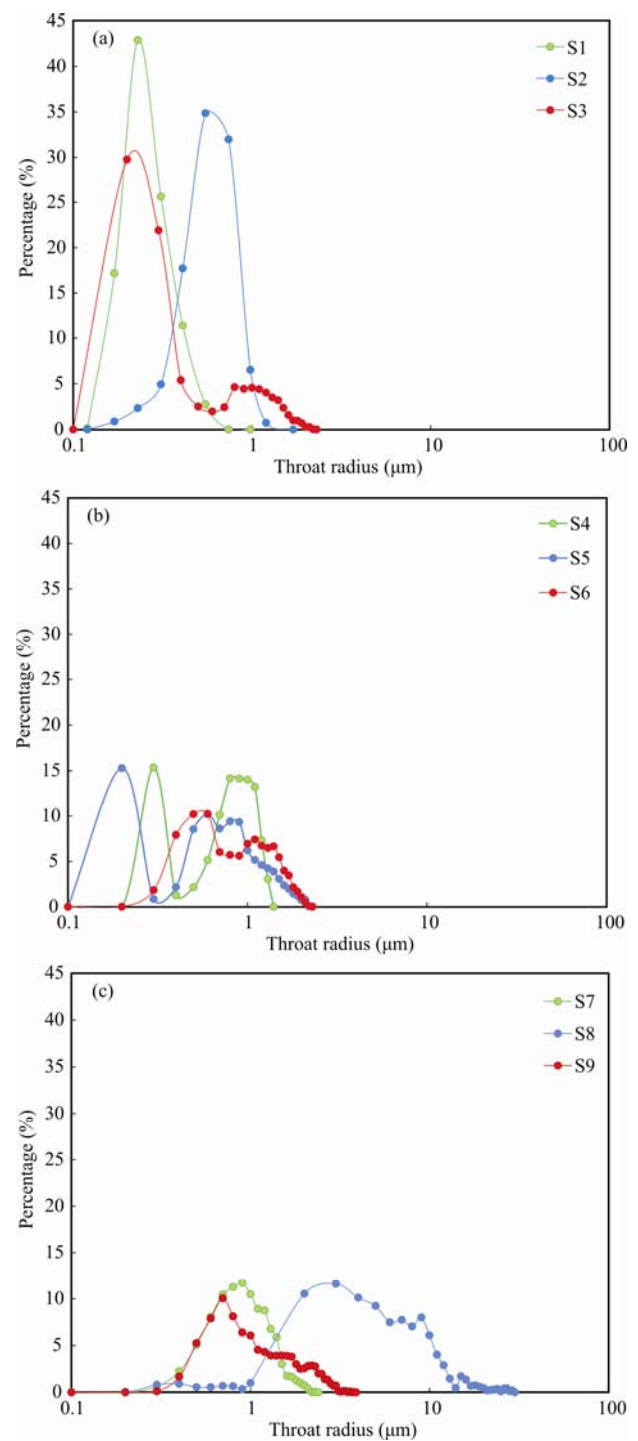


Fig. 10. The three types of throat radius distribution curves of the nine samples. The shapes of the curves show the different characteristics, such as size range and central tendency.

However, there exhibit significant differences in the curves of gas-phase relative permeability: (1) the curves of the type-I samples are in an approximately linear shape (Fig. 11a); (2) the curves of the type-II samples are concave at high water saturation and tend to a line with the decrease in water saturation (Fig. 11b); (3) the curves of the type-III samples are concave (Fig. 11c).



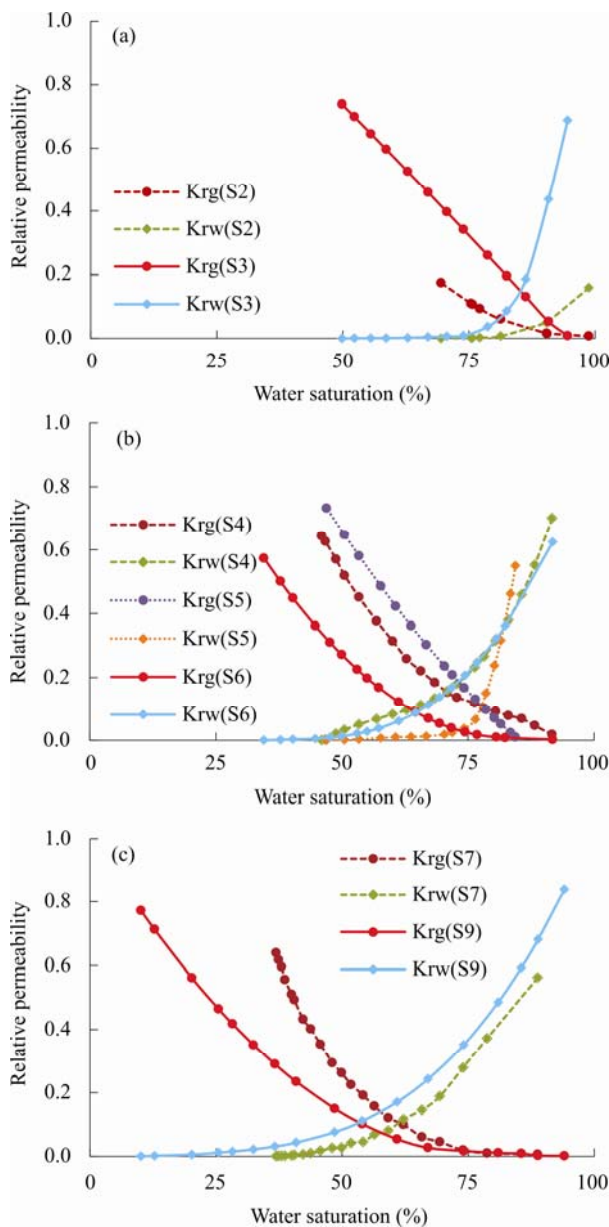


Fig. 11. Gas-water relative permeability curves obtained from the experimental data of the seven samples.

5 Discussions

5.1 Effects of pore-throat combination types on the gas-water relative permeability

The differences in the gas-water relative permeability

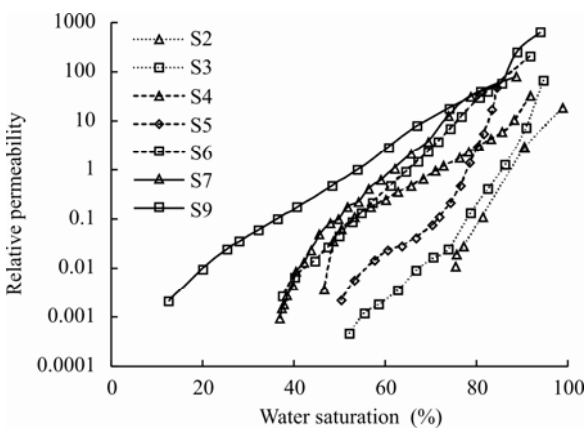


Fig. 12. Curves of  $K_{rw}/K_{rg}$  in the two-phase saturation zone obtained from the experimental data of the seven samples.

response to sandstones with three pore-throat combination types can be shown in the curves of  $K_{rw}/K_{rg}$  in the two-phase saturation zone (Fig. 12). The value on the X-axis corresponding to the left end point of the curve is  $S_{wo}$  and the length of the curve projected to the X-axis is the range of the two-phase saturation zone. The slope of the curve indicates the gas-phase flow ability under the influence of the water phase: the smaller the slope is, the stronger the gas-phase flow ability is. The results show that from type-I to type-III sandstones, the  $S_{wo}$  decreased and the two-phase saturation zone increased; furthermore, the slope of the curves decreased, indicating that the gas relative flow ability increased.

Figure 13a shows a decreasing trend in the  $S_{wo}$  of sandstones with an increase of average radius of pore and throat. Additionally, the correlation with throat radius is stronger. Wu et al. (2016) proposed that water adsorbed on flat surfaces of large pores and capillary held water in small pores or in corners of large pores can be reclassified as irreducible water when pores are considered to be capillary tubes in porous rocks. The previous study suggested that the thickness of irreducible water in pores is mainly controlled by wettability and roughness of the pore surfaces (Meybodi et al., 2011; Kibbey, 2013). Luo et al. (2015) also proved the  $S_{wo}$  is associated with hydrophilicity and pore-throat structures (size and connectivity) of the rocks, and the higher value indicates stronger hydrophilicity, smaller radius and more complicated pore-throat structures. The combination type of intercrystalline micropores and cluster throats in type-I sandstones may be the reason for the high  $S_{wo}$ . The

Table 3 Characterization parameters obtained from the gas-water relative permeability experiment of seven samples

| Type | Samples | Porosity (%) | $K_g$ (mD) | $K_w$ (mD) | $S_{wo}$ (%) | $K_{rg}(S_{wo})$ (mD) | $\frac{K_{rg}=K_{rw}}{S_{we}(\%) \quad K_{rg}(\text{mD})}$ |      | Range of two-phase saturation zone (%) |
|------|---------|--------------|------------|------------|--------------|-----------------------|--|------|--|
|      |         |              |            |            |              |                       |  |      |  |
| I    | S2      | 8.8          | 0.214      | 0.0003     | 69.47        | 0.1745                | 87   | 0.03 | 23.38                                  |
| I    | S3      | 7.2          | 0.232      | 0.0146     | 49.82        | 0.7393                | 85   | 0.15 | 23.96                                  |
| II   | S4      | 7.8          | 0.3363     | 0.0476     | 46.01        | 0.6434                | 71   | 0.16 | 42.87                                  |
| II   | S5      | 7.2          | 0.4406     | 0.0233     | 46.99        | 0.7322                | 76   | 0.07 | 26.70                                  |
| II   | S6      | 9.1          | 0.454      | 0.0364     | 34.57        | 0.5729                | 65   | 0.08 | 37.68                                  |
| III  | S7      | 7.1          | 0.5534     | 0.0217     | 36.95        | 0.6397                | 61   | 0.1  | 51.82                                  |
| III  | S9      | 4.7          | 0.892      | 0.0392     | 10.12        | 0.7721                | 54   | 0.11 | 81.25                                  |

Note:  $K_g$ , gas permeabilities;  $K_w$ , water permeabilities;  $S_{wo}$ , irreducible water saturation;  $K_{rg}(S_{wo})$ , gas relative permeabilities at irreducible water saturation;  $S_{we}$ , water saturation at the point where the gas relative permeabilities and water relative permeabilities are equal.

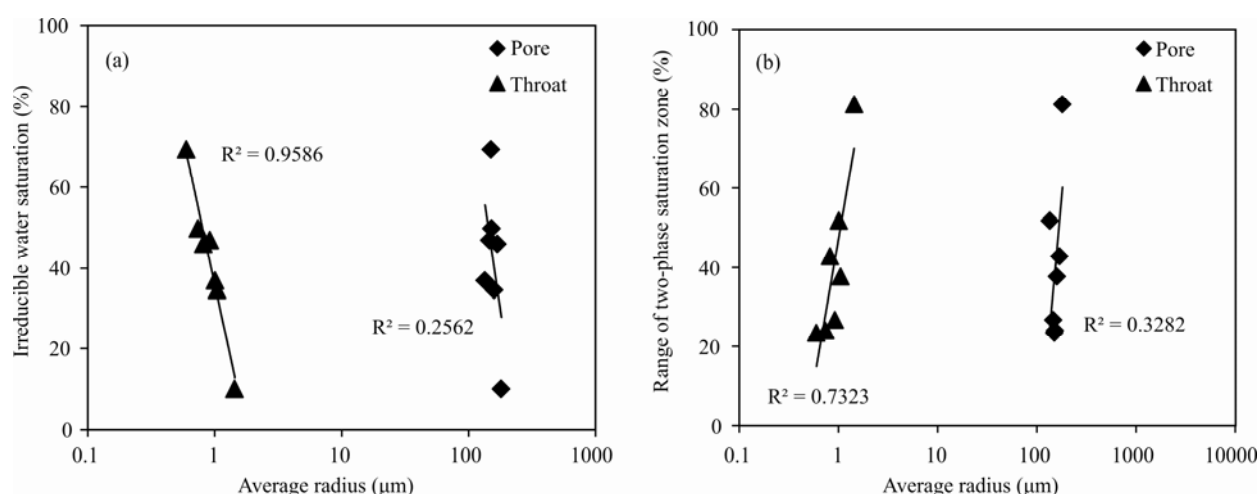


Fig. 13. The relationship between  $S_{wo}$ , the range of the two-phase saturation zone and the average radius of pore and throat.

connectivity; thus, the water phase had a larger influence on the gas-phase flow. As a result, the gas-phase relative permeability increased at a constant speed with the decrease in water saturation in both the gas-single-phase and two-phase saturation zone (Fig. 11a). In type-II and type-III samples, the major channel, such as primary intergranular pores and dissolution pores, was occupied by the water phase when the water saturation was high and would be first displaced by the gas phase due to the larger size and good connectivity. Along with the gradual connection and expansion of the pore-throat network, the slope of the gas-phase relative permeability curve gradually increased (Figs. 11b, c). However, there are also more intercrystalline micropores and cluster throats in type-II samples, which would be occupied by the water phase with the decrease in water saturation. The residual water had a larger influence on the gas relative permeability, which caused the slope of the gas-phase relative permeability curve is difficult to increase (Fig. 11b). Thus, the curves of the type-II samples tend to a line with the decrease in water saturation.

## 5.2 Diagenetic control on the pore-throat combination types

The diagenesis and porosity evolution analysis of the sandstones with three pore-throat combination types in the Zizhou area indicate that the major diagenesis affecting porosity evolution history of sandstones are compaction, dissolution and cementation. Moreover, the content of the primary pores reserved after compaction plays a dominant role in the later dissolution and cementation, which is determined by the composition of the detrital grains in sandstones. The porosity evolution of three types sandstones is summarized in Fig. 14, which proves that the pore-throat combination type in sandstones is the cumulative expression of diagenetic modifications with strong heterogeneity.

Type-III samples are mainly coarse-grained quartz arenites (Fig. 15). Due to the high content of rigid grains (Fig. 16a), sandstones can effectively resist compaction and keep the primary pores reserved. The primary

intergranular pores provide the main channel for the migration of pore water (Surdam et al., 1989; Barth and Bjørlykke, 1993), which is beneficial to form the secondary intergranular pores. Slice-shaped throats occurred along cleavages between the rigid grain margins. The rigid grains observed in the samples consist of quartz and volcanic rock fragments, between which the cleavages are regular and easily enlarged into fractures, thus forming slice-shaped throats (Fig. 6i). Quartz overgrowth generally occurs around detrital quartz grains (Pittman and Lumsden, 1968), and the throats can remain in the form of slice-shapes in this case (Fig. 16b). Nevertheless, slice-shaped throats were not observed between the detrital grains tightly cemented by quartz. Synsedimentary tephra fills the original intergranular spaces, which can form large dissolved pores due to the subsequent strong dissolution. When the tephra is almost completely dissolved in samples, pore-shrinking throats and neck-contracted throats occurred, with large throat sizes (Figs. 6j, k). However, the decrease in the throat size and the change in the throat shape occur when the cement fills the dissolution pores in the subsequent diagenetic evolution.

Type-II samples are mainly coarse-grained sublitharenites (Fig. 15). Compared with quartz arenites, the content of ductile grains (e.g., schist, phyllite, argillite, mudrock and mica) in sublitharenites is relatively high (Fig. 16a). During compaction, the rearrangement and deformation of ductile grains lead to substantial loss of primary porosity (Lundegard, 1992). Restricted migration of pore water results in weak dissolution and near-precipitation of dissolved products (Giles et al., 1990). The sandstones mainly form secondary intragranular pores and a small amount of secondary intergranular pores, and the dissolved pores are generally filled with quartz and clay mineral cement. Due to the weak dissolution and strong cementation, the types of throats depend on the types of cement. The throats occur as slice-shaped with the filling of euhedral quartz and as cluster throats with the filling of clay minerals (Figs. 16b, 6e).

Type-I samples are mainly medium-grained sublitharenites (Fig. 15). Sandstones have experienced

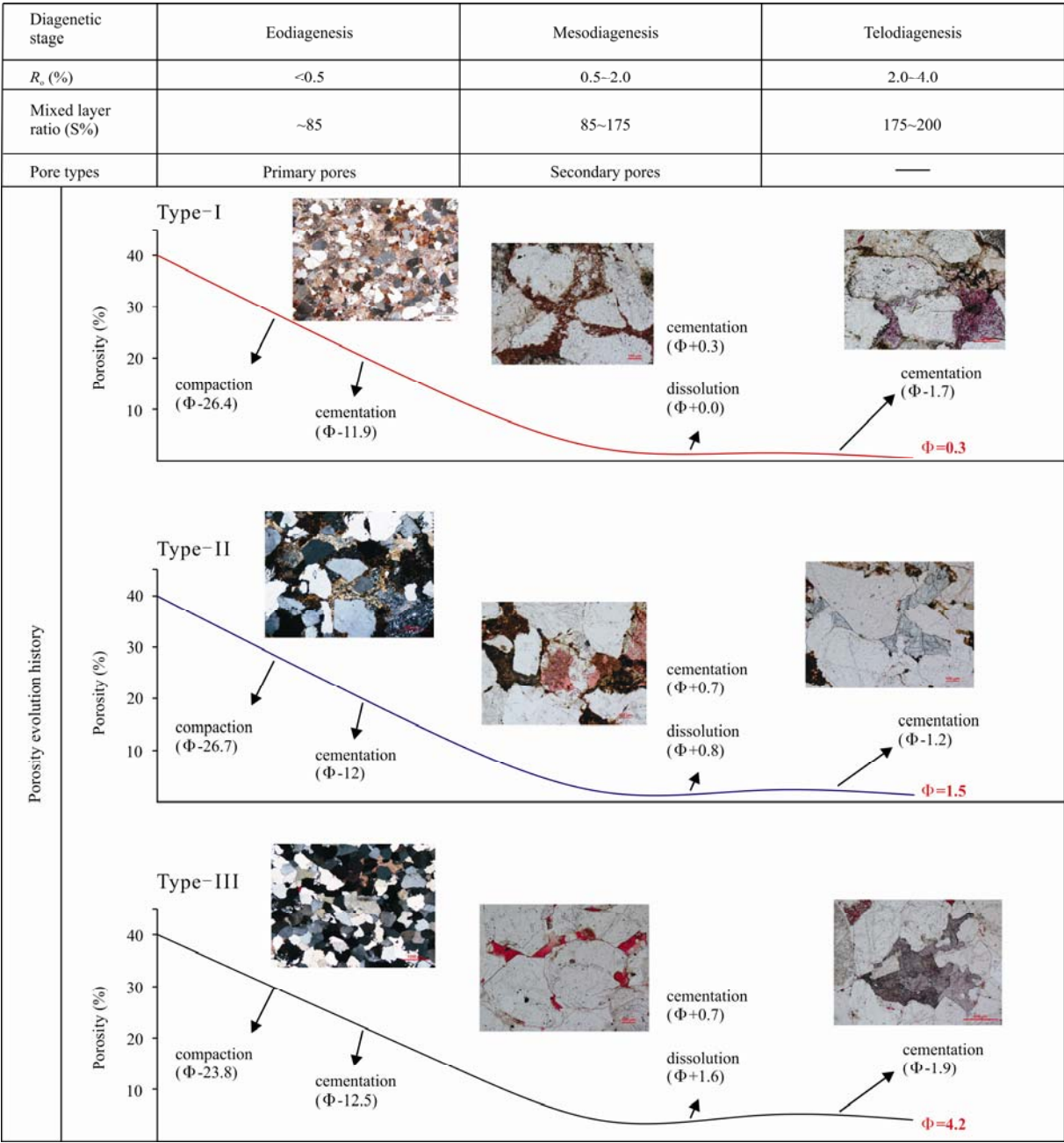


Fig. 14. Porosity evolution history of sandstones with three pore-throat combination types in Zizhou area. Data are obtained from thin-section petrography observation of 222 samples. The original porosity of well-sorted sandstone in the study area is assumed to be 40% (Houseknecht, 1987).

micropores increase the specific surface area of the reservoirs and a smaller pore-throat radius will block the gas-phase flow, which have caused the higher  $S_{wo}$  in type-I sandstones. Conversely, the water mainly exists in the movable form in the center of the large pores (Kumar et al., 2009; Kibbey, 2013); thus,  $S_{wo}$  is lower in type-II and type-III sandstones with larger pores and throats.

The range of the two-phase saturation zone is positively correlated with the average radius of pore and throat (Fig. 13b). The fact that multi-phase flows in rocks are controlled by the pore geometry and the gas-water spatial

distribution has been proved in the previous study (Anderson, 1987., Jerauld and Salter, 1990; Nicholl et al., 2000). Due to the differences in gas-water spatial distribution caused by various pore-throat types, the water-phase had different intensities of the interference effect on the gas-phase for the three types of samples, which caused the differences in the gas-phase flow ability. Thus, the curves of the gas-phase relative permeability have different slope characteristics. In type-I sandstone, water was mainly distributed in the intercrystalline micropores and cluster throats with smaller sizes and poor

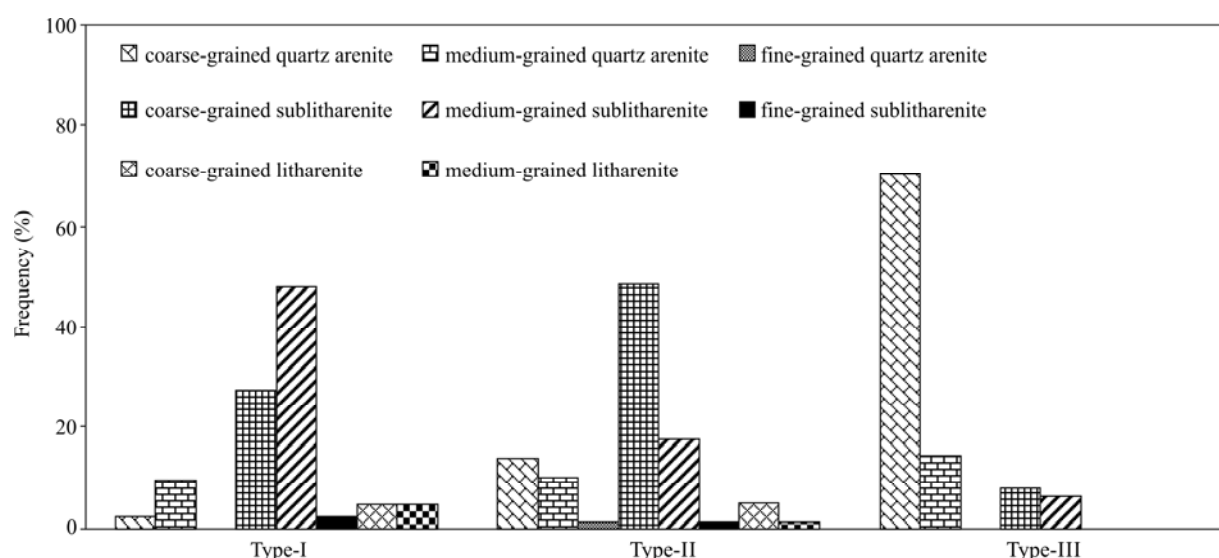


Fig. 15. Distribution of the lithology in sandstones with three pore-throat combination types in Zizhou area.

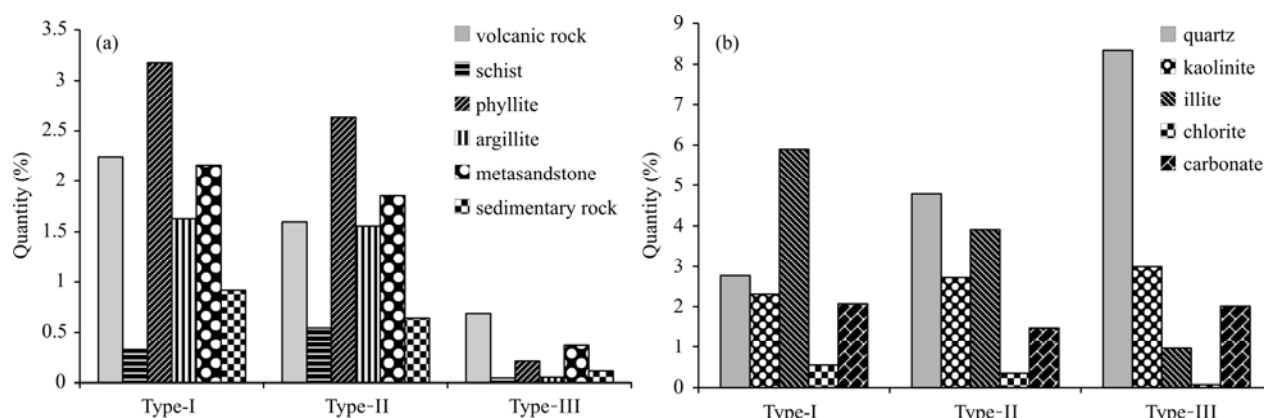


Fig. 16. Contents of (a) major rock fragments and (b) cement derived from thin-section petrography in samples with three pore-throat combination types in Zizhou area. The carbonate cement in the samples consist of calcite, siderite, Fe-calcite and ankerite.

strong compaction due to the high content of ductile grains (Fig. 16a). The loss of primary pores is not conducive to the migration of pore water, and the rare occurrence of dissolved pores in sandstones indicates that the contribution of dissolution to sandstones is minor. Clay minerals formed during cementation provide intercrystalline micropores, which are the main types of sandstones (Fig. 16b). The sizes and shapes of the cluster throats located in intercrystalline micropores are controlled by clay minerals. Kaolinite and illite mainly occur as cement filling in the pores and throats, which have two origins: altered from tephra and authigenically crystallized from meteoric water. Finely laminated illite observed in thin sections indicate an altered origin generally occurring with honeycomb-like pores in SEM (Fig. 6f), whereas authigenic illite has fibrous, hair-like characteristics with small and cross-capillary throats (Tian et al., 2013; Zhao et al., 2016). Kaolinite occurs as booklets and vermicular aggregates with crystals stacked in diverse directions (Fig. 6c), in which the pores are unclear to distinguish from throats. The sizes of the cluster throats in altered kaolinite are small due to the compact

stack of fine crystals from rapid crystallization (Fig. 6c). Authigenic kaolinite with a euhedral-granular texture is commonly scattered in the pores with large pore sizes and large throat sizes. (Fig. 6f). A variety of clay minerals present in the sandstones make the pore-throat structure more complicated.

## 6 Conclusions

(1) Thin-section petrology observation revealed three pore-throat combination types in tight gas sandstones in the Zizhou area. Variations in the permeability exist in sandstones with different pore-throat combination types, which indicate type-III sandstones are better reservoirs, followed by type-II sandstones and type-I sandstones.

(2) RCP results show that there are significant differences in throat radius, size range and central tendency of the three types of samples, indicating pore-throat combination types play the controlling role in the throat size distribution in sandstones.

(3) The pore-throat combination types in sandstones have important impacts on the gas-water relative



permeability. From type-I to type-III sandstones, the  $S_{wo}$  decreased and the two-phase saturation zone increased; furthermore, the slope of the curves decreased. The results indicate that the interference effect of water-phase on gas-phase decreased and the gas relative flow ability increased.

(4) The pore-throat combination types in sandstones are the cumulative expression of lithology and diagenetic modifications with strong heterogeneity. The content of the primary pores reserved after compaction plays a dominate role in the later dissolution and cementation, which is determined by the composition of the detrital grains in sandstones.

## Acknowledgements

This work was supported by the Natural Science Foundation of China (grant No. 41772130). The authors wish to acknowledge the Research Institute of Petroleum Exploration & Development of Changqing Oilfield Company for providing the drill cores and their support in completing this study.

Manuscript received Aug. 1, 2018

accepted Dec. 20, 2018

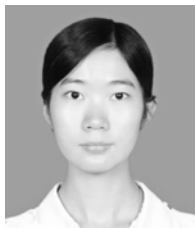
associate EIC HAO Ziguo

edited by HAO Qingqing

## References

- Anderson, W.G., 1987. Wettability literature survey Part 5: the effects of wettability on relative permeability. *Journal of Petroleum Technology*, 39: 1453–1468.
- Bai, B., Zhu, R.K., Wu, S.T., Yang, W.J., Gelb, J., Gu, A., Zhang, X.X., and Su, L., 2013. Multi-scale method of nano (micro)-CT study on microscopic pore structure of tight sandstone of Yanchang Formation, Ordos Basin. *Petroleum Exploration & Development*, 40: 354–358 (in Chinese with English abstract).
- Barth, T., and Bjørlykke K., 1993. Organic acids from source rock maturation: generation potentials, transport mechanisms and relevance for mineral diagenesis. *Applied Geochemistry*, 8 (4): 325–337.
- Bultreys, T., Stappen, J.V., Kock, T.D., Boever, W.D., Boone, M.A., Hoorebeke, L.V., and Cnudde, V., 2016. Investigating the relative permeability behavior of microporosity-rich carbonates and tight sandstones with multiscale pore network models. *Journal of Geophysical Research: Solid Earth*, 121: 7929–7945.
- Cao, F., Zou, C.N., Fu, J.H., and Yang, Z., 2011. Evidence analysis of natural gas near-source migration-accumulation model in the Sulige large gas province, Ordos Basin, China. *Acta Petrologica Sinica*, 27: 857–866 (in Chinese with English abstract).
- Chalmers, G.R., Bustin, R.M., and Power, I.M., 2012. Characterization of gas shale pore systems by porosimetry, pycnometry, surface area, and field emission scanning electron microscopy/transmission electron microscopy image analyses: examples from the Barnett, Woodford, Haynesville, Marcellus, and Doig units. *AAPG Bulletin*, 96: 1099–1119.
- Dai, J.X., Li, J., Luo, X., Zhang, W.Z., Hu, G.Y., Ma, C.H., Guo, J.M., and Ge, S.G., 2005. Stable carbon isotope compositions and source rock geochemistry of the giant gas accumulations in the Ordos Basin, China. *Organic Geochemistry*, 36: 1617–1635.
- Deng, H., Leguizamon, J., and Aguilera, R., 2011. Petrophysics of triple-porosity tight gas reservoirs with a link to gas productivity. In: *SPE Western North American Region Meeting*.
- Dou, W.C., Liu, L.F., Wu, K.J., Xu, Z.J., and Feng, X., 2017. Origin and significance of secondary porosity: a case study of Upper Triassic tight sandstones of Yanchang Formation in Ordos Basin, China. *Journal of Petroleum Science and Engineering*, 149: 485–496.
- Durucan, S., Ahsan, M., Shi, J.Q., Syed, A., and Korre, A., 2012. Two phase relative permeabilities for gas and water in selected European coals. *Fuel*, 134: 226–236.
- Er, C., Zhao, J.Z., Bai, Y.B., Wu, W.T., Zhang, J., and Wei, Z.K., 2015. Features of tight sandstone reservoir and origin of tightness: an example from Chang-7 member, Triassic Yanchang Formation in Chenghao area, Ordos Basin. *Acta Geologica Sinica (English Edition)*, 89: 25–26.
- Folk, R.L., 1980. *Petrology of sedimentary rocks*. Austin, Texas: Hemphill Publishing, 610.
- Ge, X.M., Fan, Y.R., Li, J.T., and AleemZahid, M., 2015. Pore structure characterization and classification using multifractal theory—an application in Santanghu Basin of western China. *Journal of Petroleum Science and Engineering*, 127: 297–304.
- Giles, M.R., and De Bore, R.B., 1990. Origin and significance of redistribution secondary porosity. *Marine and Petroleum Geology*, 7(4): 378–397.
- Giri, A., Tarafdar, S., Gouze, P., and Dutta, T., 2012. Fractal pore structure of sedimentary rocks: simulation in 2-D using a relaxed bidisperse ballistic deposition model. *Journal of Applied Geophysics*, 87: 40–45.
- Higgs, K.E., Zwingmann, H., Reyes, A.G., and Funnell, R.H., 2007. Diagenesis, porosity evolution, and petroleum emplacement in tight gas reservoirs, Taranaki Basin, New Zealand. *Journal of Sedimentary Research*, 77: 1003–1025.
- Hill, P.J., and Collen, J.D., 1978. The Kapuni sandstones from Inglewood-1 well, Taranaki: petrology and the effect of diagenesis on reservoir characteristics. *New Zealand Journal of Geology and Geophysics*, 21: 215–228.
- Hu, Q., Ewing, R.P., and Dultz, S., 2012. Low pore connectivity in natural rock. *Journal of Contaminant Hydrology*, 133: 76–83.
- Huoseknecht, D.W., 1987. Assessing the relative importance of compaction processes and cementation to reduction of porosity in sandstone. *AAPG Bulletin*, 71(3): 633–642.
- Jerauld, G.R., and Salter, S.J., 1990. The effect of pore-structure on hysteresis in relative permeability and capillary pressure: pore-level modeling. *Transport in Porous Media*, 5: 103–151.
- Ji, L.M., Yan, K., Meng, F.W., and Zhao, M., 2010. The oleaginous Botryococcus from the Triassic Yanchang Formation in Ordos Basin, Northwestern China: morphology and its paleoenvironmental significance. *Journal of Asian Earth Sciences*, 38: 175–185.
- Jia, C.Z., Zou, C.N., Li, J.Z., Li, D.H., and Zheng, M., 2016. Evaluation criteria, major types, characteristics and resource prospects of tight oil in China. *Petroleum Research*, 1: 1–9.
- Johnson, E.F., Bossler, D.P., and Naumann, V.O., 1959. Calculation of relative permeability from displacement experiments. *Petroleum Transactions, AIME*, 216: 370–372.
- Kibbey, T.C.G., 2013. The configuration of water on rough natural surfaces: Implications for understanding air–water interfacial area, film thickness, and imaging resolution. *Water Resources Research*, 49: 4765–4774.
- Kumar, M., Sok, R., Knackstedt, M., Latham, S., Senden, T.J., Sheppard, A.P., Varslot, T., and Arns, C., 2010. Mapping 3D pore scale fluid distributions: how rock resistivity is influenced by wettability and saturation history. *Petrophysics*, 51: 102–117.
- Lai, J., Wang, G.W., Chai, Y., Ran, Y., and Zhang, X.T., 2015. Depositional and diagenetic controls on pore structure of tight gas sandstone reservoirs: evidence from Lower Cretaceous Bashijiqike Formation in Kelasu thrust belts, Kuqa depression in Tarim Basin of west China. *Resource Geology*, 65: 55–75.
- Lander, R.H., and Walderhaug, O., 1999. Predicting porosity through simulating sandstone compaction and quartz cementation. *AAPG Bulletin*, 83: 433–449.
- Li, P., Zheng, M., Bi, H., Wu, S.T., and Wang, X.R., 2017. Pore throat structure and fractal characteristics of tight oil sandstone: a case study in the Ordos Basin, China. *Journal of Petroleum Science and Engineering*, 149: 665–674.
- Liu, H.L., Yang, Y.Y., Wang, F.Q., Deng, X.Q., Liu, Y., Nan, J.X., Wang, J., and Zhang, H.J., 2018. Micro pore and throat

- characteristics and origin of tight sandstone reservoirs: a case study of the Triassic Chang 6 and Chang 8 members in Longdong area, Ordos Basin, NW China. *Petroleum Exploration and Development*, 45: 223–234 (in Chinese with English abstract).
- Liu, M.J., Liu, Z., Wang, P., and Pan, G.F., 2016. Diagenesis of the Triassic Yanchang Formation tight sandstone reservoir in the Xifeng-Ansai of Ordos Basin and its porosity evolution. *Acta Geologica Sinica* (English Edition), 90: 956–970.
- Liu, X.F., Wang, J.F., Ge, L., Hu, F.L., Li, C.L., Li, X., Yu, J., Xu, H.J., Lu, S.F., and Xue, Q.Z., 2017. Pore-scale characterization of tight sandstone in Yanchang Formation Ordos Basin China using micro-CT and SEM imaging from nm– to cm–scale. *Fuel*, 209: 254–264.
- Lundegard, P.D., 1992. Sandstone porosity loss– a “big picture” view of the importance of compaction. *Journal of Sedimentary Research*, 62: 250–260.
- Luo, S.S., Peng, Y.H., Wei, X.S., Zheng, A.L., Shao, Y., Wei, W., and Lv, Q.Q., 2015. Characteristics and classification of gas-water relative permeability curves of tight sandstone reservoirs in Sulige Gas Field. *Journal of Xi'an University* (Natural Science Edition), 30: 55–61 (in Chinese with English abstract).
- Lv, Z.X., and Liu, S.B., 2009. Ultra-tight sandstone diagenesis and mechanism for the formation of relatively high-quality reservoir of Xujiache Group in western Sichuan. *Acta Petrologica Sinica*, 25: 2373–2383 (in Chinese with English abstract).
- Meybodi, H.E., Kharrat, R., and Wang, X., 2011. Study of microscopic and macroscopic displacement behaviors of polymer solution in water-wet and oil-wet media. *Transport in Porous Media*, 89: 97–120.
- Morad, S., Al-Ramadan, K., Ketzer, J.M., and DeRos, L.F., 2010. The impact of diagenesis on the heterogeneity of sandstone reservoirs: a review of the role of depositional facies and sequence stratigraphy. *AAPG Bulletin*, 94: 1267–1309.
- Nelson, P.H., 2009. Pore-throat sizes in sandstones, tight sandstones, and shales. *AAPG Bulletin*, 93: 329–340.
- Nicholl, M.J., Rajaram, H., and Glass, R.J., 2000. Factors controlling saturated relative permeability in a partially-saturated horizontal fracture. *Geophysical Research Letters*, 27: 393–396.
- Pittman, E.D., 1992. Relationship of porosity and permeability to various parameters derived from mercury injection: capillary pressure curves for sandstone. *AAPG Bulletin*, 76: 191–198.
- Pittman, E.D., and Lumsden, D.N., 1968. Relationship between chlorite coatings on quartz grains and porosity. *Journal of Sedimentary Research*, 38: 668–670.
- Rezaee, R., Saeedi, A., and Clennell, B., 2012. Tight gas sands permeability estimation from mercury injection capillary pressure and nuclear magnetic resonance data. *Journal of Petroleum Science & Engineering*, 88–89: 92–99.
- Shan, X., Yu, X.H., Han, X.Q., Clift, P., Zhou, J.S., Du, Y.H., Li, Y.L., Su, D.X., and Jin, L., 2018. Sedimentology and sequence stratigraphy of marine to lacustrine, deltaic deposits in a craton basin and their controlling factors: Shan 2 member–He 8 member (Guadalupian–Lopingian, Permian), southeast Ordos Basin, North China. *Acta Geologica Sinica* (English Edition), 92(1): 268–285.
- Shanley, K.W., Cluff, R.M., and Robinson, J.W., 2004. Factors controlling prolific gas production from low-permeability sandstone reservoirs: implications for resource assessment, prospect development, and risk analysis. *AAPG Bulletin*, 88: 1083–1121.
- Sheng, J., Xu, L., Wang, Q., Yang, C., Ding, X.J., Liu, Y.N., 2018. The seepage characteristics of different pore types of tight sandstone gas reservoir–Taking the Southeast area of Silige gas field, Ordos basin as an example. *Geological Review*, 64(3): 764–776.
- Spencer, C.W., 1985. Geologic aspects of tight gas reservoirs in the Rock Mountain region. *Journal of Petroleum Technology*, 37: 1308–1314.
- Surdam, R.C., Crossey, L.J., Hagen, E.S., Heasler, H.P., 1989. Organic-inorganic interactions and sandstones diagenesis. *AAPG Bulletin*, 73(1): 1–23.
- Teige, G.M.G., Thomas, W.L.H., Hermanrud, C., Oren, P.E., Rennan, L., Wilson, O.B., and Bolas, H.M.N., 2006. Relative permeability to wetting-phase water in oil reservoirs. *Journal of Geophysical Research Solid Earth*, 111(B12204): 1–20.
- Tian, J.F., Gao, Y.L., Zhang, P.B., Wang, X.J., and Yang, Y.Y., 2013. Genesis of illite in Chang7 tight oil reservoir in Heshui area, Ordos Basin. *Oil & Gas Geology*, 34, 700–707 (in Chinese with English abstract).
- Wu, F., Fan, Q.C., Huang, D., Ma, L., Liang, X.Y., and Sima, L., 2016. Predicting gas-water relative permeability using nuclear magnetic resonance and mercury injection capillary pressure measurements. *Journal of Natural Gas Science & Engineering*, 32: 35–47.
- Wu, H., Ji, Y.L., Liu, R.E., Zhang, C.L., and Chen, S., 2017. Insight into the pore structure of tight gas sandstones: a case study in the Ordos Basin, NW China. *Energy & Fuels*, 31: 13159–13178.
- Wu, H., Zhang, C.L., Ji, Y.L., Liu, R.E., Wu, H., Zhang, Y.Z., Geng, Z., Zhang, Y.L., and Yang, J.Q., 2018. An improved method of characterizing the pore structure in tight oil reservoirs: integrated NMR and constant-rate-controlled porosimetry data. *Journal of Petroleum Science & Engineering*, 166: 778–796.
- Xi, K., Cao, Y., Haile, B.G., Zhu, R., Jahren, J., Bjørlykke, K., Zhang, X., and Hellevang, H., 2016. How does the pore-throat size control the reservoir quality and oiliness of tight sandstones? the case of the Lower Cretaceous Quantou Formation in the southern Songliao Basin, China. *Marine and Petroleum Geology*, 76: 1–15.
- Xiao, D.S., Jiang, S., Thul, D., Huang, W.B., Lu, Z.Y., and Lu, S.F., 2017. Combining rate-controlled porosimetry and NMR to probe full-range pore throat structures and their evolution features in tight sands: a case study in the Songliao Basin, China. *Marine & Petroleum Geology*, 83: 111–123.
- Xiao, D.S., Lu, S.F., Lu, Z.Y., Huang, W.B., and Gu, M.W., 2016. Combining nuclear magnetic resonance and rate-controlled porosimetry to probe the pore-throat structure of tight sandstones. *Petroleum Exploration and Development*, 43: 961–970 (in Chinese with English abstract).
- Yu, J.W., Ye, Y., Liu, N., Zhu, Y.C., and Wen, H.G., 2018. Character differences and controlling factors of reservoirs in the Upper-Middle Jurassic Fudong slope area, Junggar Basin. *Acta Geologica Sinica*, 92(5): 1070–1080 (in Chinese with English abstract).
- Yu, X.H., 2009. *Basis of Hydrocarbon Reservoir Geology*. Beijing: Petroleum Industry Press, 393 (in Chinese).
- Zhang, X.Y., Wu, C.F., and Liu, S.X., 2017. Characteristic analysis and fractal model of the gas-water relative permeability of coal under different confining pressures. *Journal of Petroleum Science & Engineering*, 159: 488–496.
- Zhao, H., Ning, Z., Wang, Q., Zhang, R., Zhao, T., Niu, T., and Zeng, Y., 2015. Petrophysical characterization of tight oil reservoirs using pressure-controlled porosimetry combined with rate-controlled porosimetry. *Fuel*, 154: 233–242.
- Zhao, H.W., Ning, Z.F., Zhao, T.Y., Zhang, R., and Wang, Q., 2016. Effects of mineralogy on petrophysical properties and permeability estimation of the Upper Triassic Yanchang tight oil sandstones in Ordos Basin, northern china. *Fuel*, 186: 328–338.
- Zou, C.N., Tao, S.Z., Han, W.X., Zhao, Z.Y., Ma, W.J., Li, C.W., Bai, B., and Gao, X.H., 2018. Geological and geochemical characteristics and exploration prospect of coal-derived tight sandstone gas in China: case study of the Ordos, Sichuan and Tarim Basins. *Acta Geologica Sinica* (English Edition), 92: 1609–1626.
- Zou, C.N., Yang, Z., Zhu, R.K., Zhang, G.S., Hou, L.H., Wu, S.T., Tao, S.Z., Yuan, X.J., Dong, D.Z., Wang, Y.M., Wang, L., Huang, J.L., and Wang, S.F., 2015. Progress in China's unconventional oil & gas exploration and development and theoretical technologies. *Acta Geologica Sinica* (English Edition), 89: 938–971.

**About the first author**

LI Mi, female, born in 1994 in Xi'an City, Shaanxi Province, is now a Ph. D candidate of the China University of Mining & Technology. Her research field is unconventional petroleum reservoir sedimentology. E-mail: 15996944776 @ 163.com.

**About the corresponding author**

GUO Yinghai, male, born in 1963 in Xingtai City, Hebei Province; a professor of the China University of Mining & Technology, is mainly engaged in researches and teaching work of coalfield, petroleum geology and exploration. E-mail: gyhai@163.com.